Available online at www.sciencedirect.com
ScienceDirect
Journal of Molecular Catalysis A: Chemical 265 (2007) 195–204
JOURNAL OF MOLECULAR CATALYSIS A: CHEMICAL
www.elsevier.com/locate/molcata

Effect of crystallinity on the catalytic performance of amorphous Co–B particles prepared from cobalt nitrate and potassium borohydride in the cinnamaldehyde hydrogenation

Dong-Ge Tong [a,*], Wei Chu [a,*], Yong-Yue Luo [b], Xiao-Yang Ji [c], Yi He [c]

[a] *Lab 230, College of Chemical Engineering, Sichuan University, Chengdu 610065, China*
[b] *State Key Laboratory of Polymer Materials, Sichuan University, Chengdu 610065, China*
[c] *Analytic and Testing Center, Sichuan University, Chengdu 610064, China*

Received 19 September 2006; received in revised form 13 October 2006; accepted 16 October 2006
Available online 20 October 2006

Abstract

The amorphous Co–B particles were prepared from cobalt nitrate and potassium borohydride. Ethanol-thermal treatment has been used to promote the crystallinity of Co–B particles. Both the amorphous and crystallized Co–B particles were characterized by X-ray powder diffraction (XRD), scanning electron micrograph (SEM), inductively coupled plasma (ICP), X-ray photoelectron spectroscopy (XPS), specific surface area (S_{BET}), CO temperature-programmed desorption (TPD), and magnetic performance test. After crystallization, the synergistic effect between Co and B, the structure stability, and the magnetic property of Co–B enhanced while the activation energy in cinnamaldehyde (CMA) hydrogenation decreased. Furthermore, the conversion of cinnamaldehyde (CMA) increased from 5% to 57%. The hydrogenation of the C=C bond in cinnamaldehyde (CMA) is favored for the amorphous Co–B particles while the hydrogenation of the C=O bond is preferred for the crystallized Co–B particles. After 13 cycles, the crystallized Co–B particles remain higher cinnamaldehyde (CMA) conversion and cinnamyl alcohol (CMO) selectivity, which is attributed to their good structure stability and the novel magnetic method for recycle; while the cycle performance of amorphous Co–B particles is poor due to their instable structure.
© 2006 Elsevier B.V. All rights reserved.

Keywords: Amorphous Co–B particles; Cinnamaldehyde; Hydrogenation; Crystallization; Magnetic properties

1. Introduction

Amorphous alloys have been extensively studied in the past 50 years due to their excellent electronic, magnetic and surface properties [1,2]. Recently, amorphous alloy, such as Ni–B, Co–B, etc., has been reported as a powerful catalyst in selective hydrogenation [3,4]. The majority of published research has concentrated on the effect of different supports, and the addition of second metals on the selectivity of the catalysts for selective hydrogenation. However, there are few reports for the effect of the crystallinity on the hydrogenation performance for amorphous alloy catalysts despite crystallinity is an important factor for the material properties. It is possibly attributed to the difficulty in promotion the crystallinity of amorphous alloy particles without occurrences of decomposition or side reaction [1,2]. Meanwhile, for unsupported amorphous alloy catalyst, the recycle problem is distinct [5]. To our best knowledge, there is no report for recycle of amorphous alloy catalyst by using magnetic method.

In this paper, amorphous Co–B particles were firstly synthesized by chemical reduction of cobalt nitrate by potassium borohydride. A novel technique named low temperature ethanol-thermal treatment, which replaced H_2O with ethanol in the hydrothermal method, has been developed in order to prompt the crystallinity of Co–B particles. Amorphous and crystallized Co–B particles were examined as catalysts for cinnamaldehyde (CMA) hydrogenation. The effect of crystallinity on activation energy, hydrogenation mechanism, and cycle performance of Co–B particles was investigated. Furthermore, the effect of crystallinity on the magnetic properties of Co–B particles was also

* Corresponding authors. Tel.: +86 28 8540 0591/3836; fax: + 86 28 8540 3397.
E-mail addresses: tongdongge@163.com (D.-G. Tong), chuwei65@yahoo.com.cn (W. Chu).

1381-1169/$ – see front matter © 2006 Elsevier B.V. All rights reserved.
doi:10.1016/j.molcata.2006.10.032

studied in order to develop a simple, economic magnetic method for recycling Co–B.

2. Experimental

2.1. Catalyst preparation

Amorphous Co–B particles were prepared as follows. All the reagents were of analytical grade. Twenty millilitres cobalt nitrate (0.5 mol/L) aqueous solution was added to potassium borohydride aqueous solution (20 mL of 2 mol/L), which containing 0.2 mol/L NaOH at ice-bath. The dropping rate was 2.5 mL/min. A stirring (200 rpm) was kept throughout the reaction using a magnetic stirrer. When no bubbles were released, the black precipitate was washed with distilled water three times, followed by ethanol three times. Finally, the sample was stored in absolute ethanol until the time of use.

In order to prompt the crystallinity of Co–B particles without occurrences of phase decomposition and side reaction, low temperature ethanol-thermal treatment technique has been developed. The typical experimental procedure is described as follows. The desired amounts of Co–B particles and absolute ethanol were added in a 100 mL stainless autoclave equipped with a magnetic stirrer and an electric heating system. Then the reactor was sealed and filled repetitively with H_2 more than four times to exclude air. Then it was filled H_2 up to 4.2 MPa in order to protect the Co–B particles from oxidation during the treatment, followed by heating slowly (80 K/h) until 353 K (slightly higher than the boiling point of ethanol). After treatment for 12 h, the sample was collected and then stored in absolute ethanol until the time of use.

2.2. Characterization

X-ray diffraction (XRD) patterns of the samples were acquired on D/rmax-rA X-ray diffractometer with Cu Kα sources. During the characterization, the ethanol wet Co–B sample was used and dried in situ in the atmosphere of Ar (purity of 99.99%, treated with a Chrompack clean-oxygen filter) to protect the sample from oxidation. The compositions of the samples were analyzed by inductively coupled plasma (ICP, Irris, Avantage). The surface morphologies were observed by means of a scanning electron microscopy (SEM, Hitachi, S-800). X-ray photoelectron spectroscopy (XPS) was performed on a Perkin-Elmer 5000C ESCA system using Al Kα radiation to determine the surface electronic states of Co–B particles. Similarly, the Co–B samples were also dried in situ in pure Ar atmosphere to avoid oxidation. All the binding energy (BE) values were calibrated by using C 1s = 284.6 eV as a reference. The surface composition was determined by using 0.13 and 2.50 as the sensitivity factors to B 1s and Co $2p_{3/2}$, respectively, offered by Perkin-Elmer Company [6]. The specific surface area (S_{BET}) was measured by nitrogen absorption at 77 K after degassing at 373 K for 2 h. The room temperature magnetic characterization of the sample was performed by a vibrating sample magnetometer (MagLab-12, Oxford). CO temperature-programmed desorption (TPD) was performed in the following procedure. Firstly, the air on the sample surface was removed with a nitrogen steam (purity of 99.99%, treated with a Chrompack clean-oxygen filter) at 573 K for 1 h and the surface was cooled to room temperature in the same nitrogen steam. Then, CO was pre-adsorbed by the catalyst at 383 K for 2 h. The CO steam was then replaced with the carrier gas, which was kept at 383 K for 2 h in order to purge the gaseous and physical-absorbed CO away from the catalyst surface. After the surface was cooled down to room temperature, the CO desorption was carried out by raising the temperature at a speed of 40 K/min up to 573 K, then the released CO was determined by an on-line gas chromatograph (GC) equipped with thermal conductivity detector (TCD).

2.3. Activity test

Hydrogenation of CMA was carried out in a 100 mL stainless autoclave equipped with a magnetic stirrer and an electric heating system. After addition of 4.5 mL CMA, 40.5 mL absolute ethanol, and 0.25 g catalysts, the reactor was sealed and washed with H_2 more than four times to exclude air. Then it was filled with H_2 up to 4.2 MPa, followed by heating until 353 K. Once the pressure reached a steady state, the hydrogenation reaction was initiated immediately by stirring the reaction mixture vigorously (1100 rpm). The initial rate of reaction was obtained by measuring the drop of H_2 within the first 0.5 h, from which the specific activity was calculated by using the ideal gas equation. Reaction products were analyzed on SC-200 with flame ionization detection (FID) by means of SE-30 column at 525 K with flowing N_2 as carrier gas.

3. Results and discussion

3.1. XRD patterns

Fig. 1 shows the XRD patterns of amorphous and crystallized Co–B particles, respectively. As shown in Fig. 1a, a very weak and broad diffraction peak appears at around $2\theta = 45^\circ$, which is a characteristic of typical amorphous alloy structure of Co–B particles [3], indicating amorphous structures of the Co–B

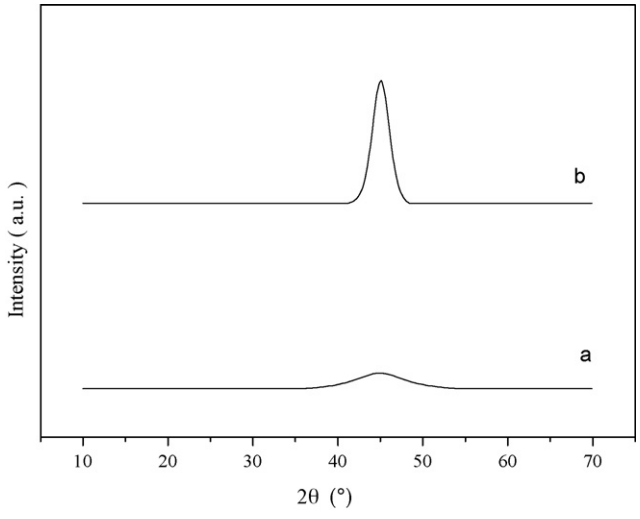

Fig. 1. XRD patterns of (a) amorphous Co–B particles; (b) crystallized Co–B particles.

Table 1
Composition and specific surface area of fresh and spent Co–B particles

Sample	Bulk composition (atom%)	Surface composition (atom%)	Specific surface area (m^2/g)
Amorphous Co–B			
Fresh	$Co_{67.9}B_{32.1}$	$Co_{62.6}B_{36.8}O_{0.6}$	131.9
4 cycles	$Co_{67.9}B_{32.1}$	$Co_{60.8}B_{39.2}$	110.7
7 cycles	$Co_{67.9}B_{32.1}$	$Co_{57.6}B_{42.4}$	92.3
9 cycles	–	–	76.8
11 cycles	$Co_{67.9}B_{32.1}$	$Co_{57.7}B_{42.3}$	62.0
Crystallized Co–B			
Fresh	$Co_{67.6}B_{32.4}$	$Co_{53.6}B_{46.4}$	70.9
4 cycles	–	–	70.6
7 cycles	$Co_{67.6}B_{32.4}$	$Co_{53.6}B_{46.4}$	70.8
9 cycles	–	–	70.5
13 cycles	$Co_{67.6}B_{32.4}$	$Co_{53.5}B_{46.5}$	70.6

particles without crystallization. After being ethanol-thermal treated at 353 K for 12 h, only a relatively sharper diffraction peak appeared in XRD patterns of the sample, indicating that the Co–B particles kept its amorphous structure with improved crystallinity. The bulk composition of Co–B particles is shown in Table 1. From Table 1, it can be seen that the bulk compositions are almost the same before and after crystallization.

From above results, one can see that low temperature ethanol-thermal treatment is an effective way to prompt the crystallinity of Co–B particles without occurrences of decomposition and side reaction.

3.2. Surface morphology and specific surface areas

Fig. 2 shows the morphology of Co–B particles before and after crystallization. As shown in Fig. 2a, the amorphous Co–B particles were composed of plenty of nano-flakes. The flower like morphology is very different from that prepared from $CoCl_2$ [3]. This difference may be attributed to the great deviation in the preparation mechanism of Co–B particles from different precursors. Because the physicochemical properties of different precursors are not the same, such as NO_3^- has a weak oxidation power under the preparation conditions in this work and the acidity of $Co(NO_3)_2$ aqueous solution is generally stronger than that of $CoCl_2$ solution, etc. The oxidation power of NO_3^- and the acidity of $Co(NO_3)_2$ aqueous solution may accelerate the reduction reaction. The accelerated reaction generate much more stronger gaseous bubbles that acted as heterogeneous nucleation centers for polycrystalline aggregation and growth of nano-flakes. The disordered nano-flakes constructed a great deal of cavities or microstructures, in which small molecules such as nitrogen could be absorbed. It also explains the much larger specific surface area of Co–B particles (131.9 m^2/g) (Table 1) without treatment in this work than that reported (26.2 m^2/g) [7].

After low temperature ethanol-thermal treatment, the nano-flakes destructed to form globe like particles that distributed homogeneously and with the average particle size around 60 nm, as shown in Fig. 2b. These were mainly attributed to the crystallization of Co–B particles as confirmed by the XRD characterization (Section 3.1). Also, the specific surface areas dramatically decreased to 70.9 m^2/g (Table 1).

3.3. XPS analysis

Figs. 3 and 4 show the Co $2p_{3/2}$ and B 1s spectra of Co–B particles before and after crystallization, respectively. The surface composition of the Co–B particles before and after treatment is listed in Table 1.

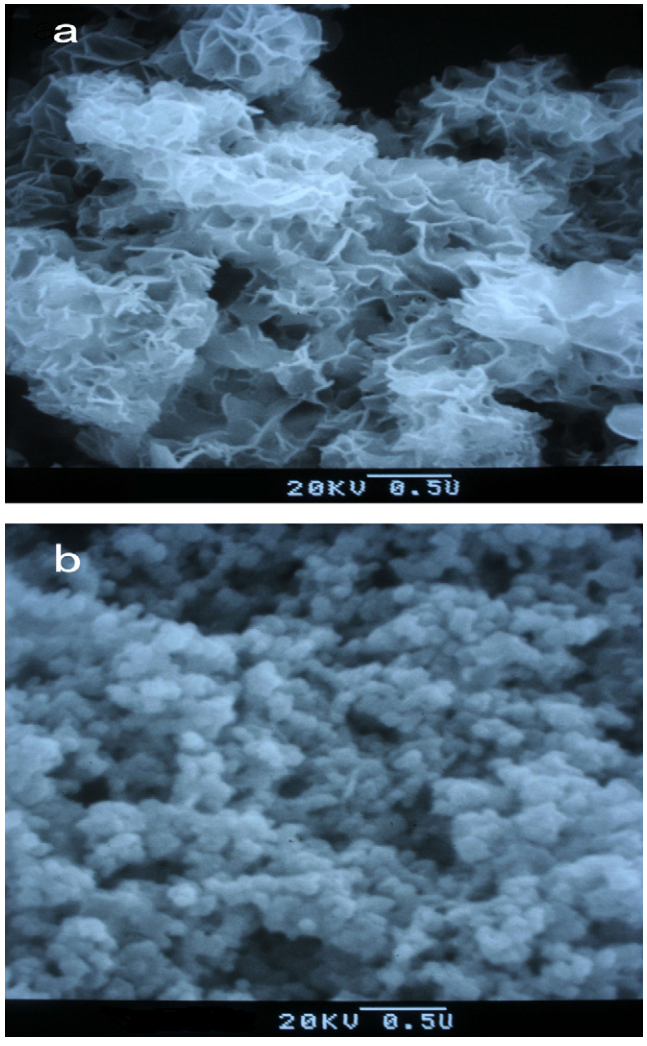

Fig. 2. Surface morphology of (a) amorphous Co–B particles; (b) crystallized Co–B particles.

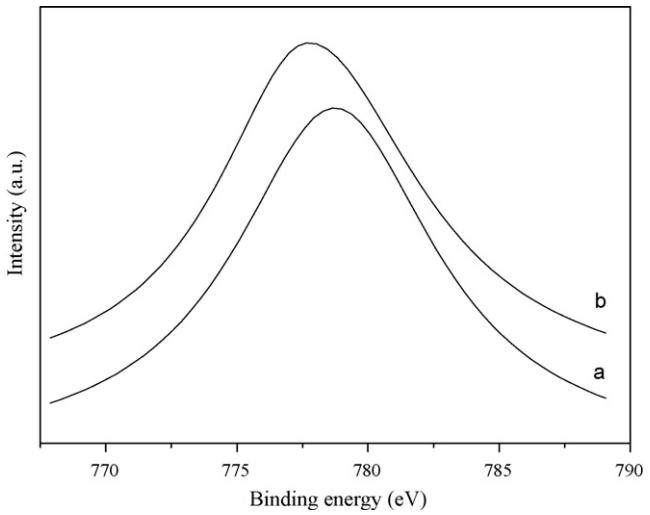

Fig. 3. Co $2p_{3/2}$ spectra of (a) amorphous Co–B particles; (b) crystallized Co–B particles.

As shown in Fig. 3a, the Co species in the Co–B sample without crystallization were present in the metallic state with the binding energy 778.6 eV [6]. But for B species, as shown in Fig. 4a, one can see that the B species were present in both the elemental state and oxidized state corresponding energies of 187.7 and 192.1 eV, respectively [6]. Contrary to the B species, no significant oxidation of the metallic Co occurred through the preparation process, indicating that the existence of the B species may effectively protect the metallic Co from oxidation. The fact that the oxidized B species could not be detected by XRD suggested that the amount of oxidized B species was small. Furthermore, the binding energy of the B species positively shifted only 0.5 eV, which is smaller in comparison with those reported (1 eV) [3,7], indicating that synergistic effect between the Co and B in the Co–B particles without crystallization is relatively weaker than those reported prepared from $CoCl_2$ [3,7]. The deviation may be attributed to the different preparation routes of Co–B particles from different precursors.

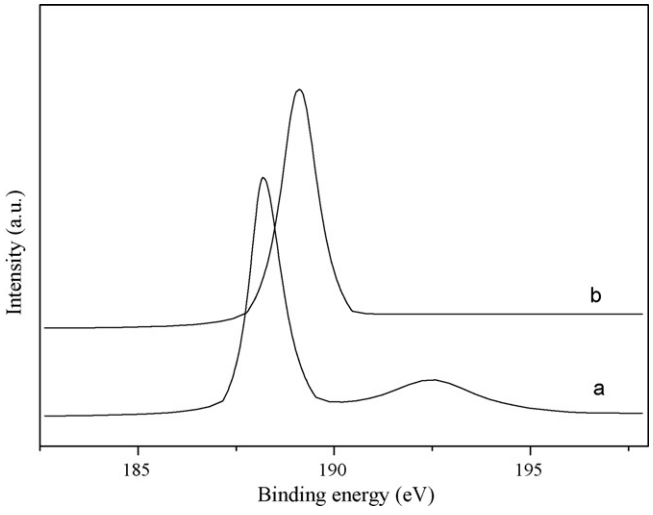

Fig. 4. B 1s spectra of (a) amorphous Co–B particles; (b) crystallized Co–B particles.

After crystallization, the peak for the metallic Co shifted to lower binding energies while the peak of the alloying B shifted positively (Fig.3b and Fig. 4b). These changes implied that the synergistic effect between Co and B enhanced. Meanwhile, the peak of those oxidized B species disappeared. The content of B on the surface of Co–B particles increased, which is presented in Table 1. The real reason is not clear and needs to be investigated intensively. The increase of alloying B atom on the surface of Co–B is also beneficial to the enhancement of synergistic effect between Co and B. The successful observation of binding energy shift for the metallic Co in this work is possibly attributed to the relatively more enrichment of B species on Co–B particles prepared from $Co(NO_3)_2$ in this work compared to those prepared from $CoCl_2$ [3,7]. Because more electrons may transfer from alloying B to the vacant d-orbital of metallic Co for Co–B particles on which surface enriched B [8].

3.4. Magnetic properties

Fig. 5a and b presents the magnetic hysteresis loops of the Co–B catalyst before and after crystallization measured at 298 K

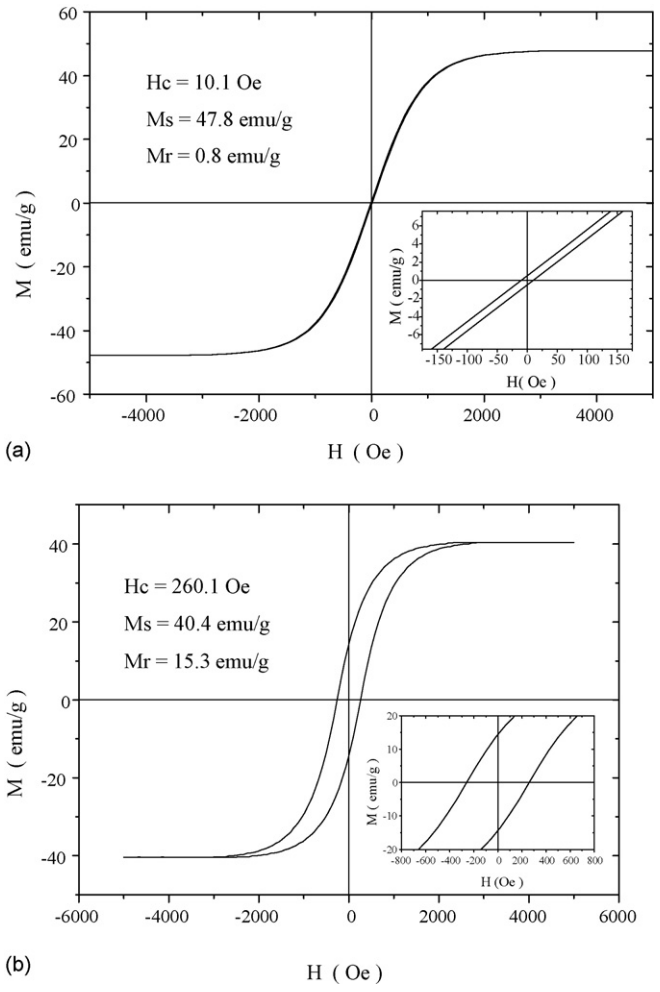

Fig. 5. Hysteresis loops of (a) amorphous Co–B particles (the inset is the full range of the hysteresis measured between −175 and 175 Oe); (b) crystallized Co–B particles at room temperature (the inset is the full range of the hysteresis measured between −800 and 800 Oe).

in an applied field of 5000 Oe, respectively. For amorphous Co–B, no significant hysteresis phenomenon was observed (Fig. 5a), revealing that the amorphous Co–B was almost superparamagnetic. This can be attributed to the particles in amorphous Co–B were so small that they might be considered to have a single magnetic domain [9]. From Fig. 5a and the enlargement of the low field data as shown in the inset, the coercivity (H_c), saturation magnetization (M_s), and remanent magnetization (M_r) could be determined to be 10.1 Oe, 47.8 emu/g, and 0.8 emu/g, respectively.

For crystallized Co–B, the typical coercivity (H_c), saturation magnetization (M_s), and remanent magnetization (M_r) at 298 K are 260 Oe, 40.4 emu/g, and 15.3 emu/g, respectively. Compared with H_c and M_r values of amorphous Co–B, the crystallized Co–B exhibited much more enhanced coercivity and remanent magnetization. It might be attributed to the increase in particle size and the increased synergistic effect between Co and B, which enhanced the total magnetic moment [10]. In addition, the M_s value of the crystallized Co–B is lower than that of amorphous Co–B. The decreased value of M_s may be resulted from the decrease in surface area after crystallization [11].

The enhanced magnetic property for crystallized Co–B enable it to be recycled by magnet, which make the recycle more easily. The simple recycle method makes the industrialization application of Co–B catalyst very promising.

3.5. Catalytic performance

3.5.1. Kinetics aspect

In order to obtain reliable kinetic data, the experimental conditions in this work were investigated in detail.

3.5.1.1. Stirring speed and catalyst amount. Mass transfer can play an important role in liquid phase hydrogenation [12]. In order to reduce the chances of mass transfer, the variation of CMA conversion over Co–B catalyst at different stirring speed and catalyst amounts were investigated, respectively (Figs. 6 and 7). From Figs. 6 and 7, it can be seen that the conversion was independent of the stirring speed in the range of 900–1200 rpm and varied linearly with catalyst amount.

In this work the stirring speed is 1100 rpm, and the catalyst mass is 0.25 g. In addition, the evaluation for internal diffusion in the CMA hydrogenation reaction over amorphous Co–B according to the method provided by Guo [12] indicated that the effect of internal diffusion in this work was negligible. So, it could be concluded that under the experimental conditions in this work, the mass transfer was significantly eliminated, and the CMA hydrogenation was controlled by the intrinsic kinetics of the reaction.

For the crystallized Co–B catalyst, under the same experimental conditions, the mass transfer was also found to be eliminated.

3.5.1.2. Hydrogen pressure and CMA concentration. The hydrogenation reaction over Co–B was performed at hydrogen pressures ranging from 2.0 to 4.2 MPa while maintaining a constant temperature (353 K) and initial CMA concentration (0.88 mol/dm^3). Fig. 8 indicates that the rate of reaction is directly proportional to the hydrogen pressure, effectively exhibiting a first-order dependency on hydrogen.

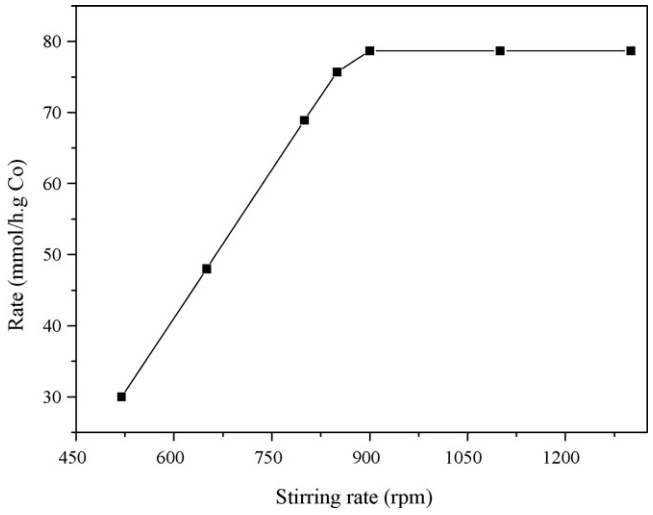

Fig. 6. Dependence of the initial hydrogenation rate over the Co–B amorphous catalyst on the stirring rate. Reaction conditions: 0.25 g catalyst, 4.5 mL CMA, 40.5 mL ethanol at $PH_2 = 4.2$ MPa and $T = 353$ K.

The effect of CMA concentration on the rate of reaction was studied at constant temperature (353 K) and initial hydrogen pressure (4.2 MPa). The result is presented in Fig. 9. The initial rates of CMA were found to be independent of CMA concentration in the range between 0.59 and 1.12 mol/dm^3. So the reaction was zero-order with respect to CMA concentration in the range between 0.59 and 1.12 mol/dm^3.

In this work the hydrogen pressure is 4.2 MPa, and the initial CMA concentration is 0.88 mol/dm^3. So, the reaction kinetics under the reaction conditions in this work can be expressed as [12]:

$$v = k[H_2][CMA]^0 \quad (1)$$

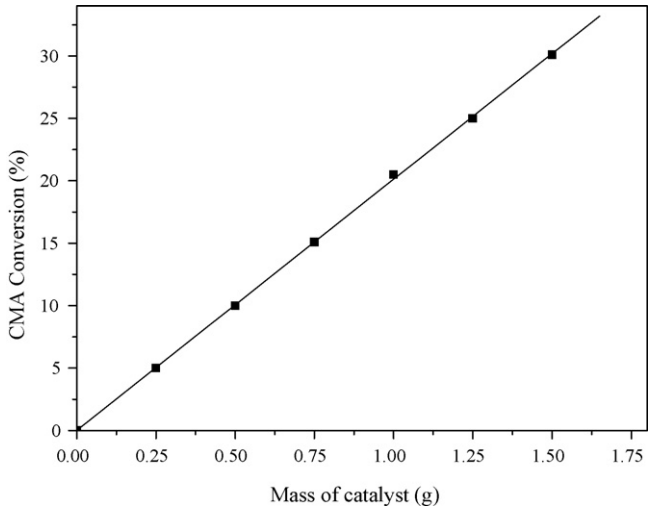

Fig. 7. Dependence of the CMA conversion on the mass of the Co–B amorphous catalyst. Reaction conditions: 4.5 mL CMA, 40.5 mL ethanol at $PH_2 = 4.2$ MPa and $T = 353$ K for 2 h. The stirring rate is 1100 rpm.

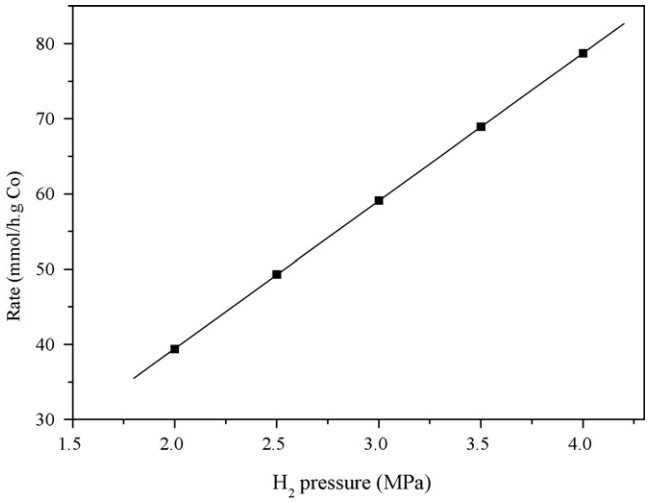

Fig. 8. Dependence of the initial hydrogenation rate over the Co–B amorphous catalyst on the hydrogen pressure. Reaction conditions: 0.25 g catalyst, 4.5 mL CMA, 40.5 mL ethanol at $T = 353$ K.

where v is the hydrogenation rate of CMA, k the reaction rate constant, and $[H_2]$ and [CMA] are the concentrations of H_2 and CMA, respectively.

Also, for the crystallized catalyst under the same conditions, the reaction kinetics was found to obey Eq. (1).

3.5.1.3. Reaction temperature. The influence of temperature on the initial specific hydrogenation uptake rates (R) for CMA hydrogenation over Co–B particles before and after crystallization was studied at 60, 75, 90, 105, and 120 °C. Fig. 10 shows that both the reactions exhibit conventional Arrhenius behavior over the temperature range from 60 to 120 °C. Based on the Arrhenius equation, the activation energy was calculated according to the slope of the straight lines obtained by plotting log R against $1/T$. The activation energy of amorphous Co–B is 25 kJ/mol. After crystallization, the activation energy decreases to 16 kJ/mol,

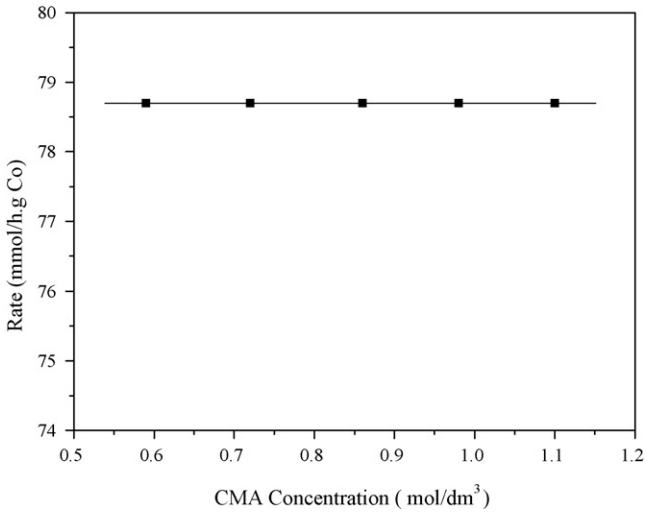

Fig. 9. Dependence of the initial hydrogenation rate over the Co–B amorphous catalyst on the CMA concentration. Reaction conditions: 0.25 g catalyst at $PH_2 = 4.2$ MPa and $T = 353$ K.

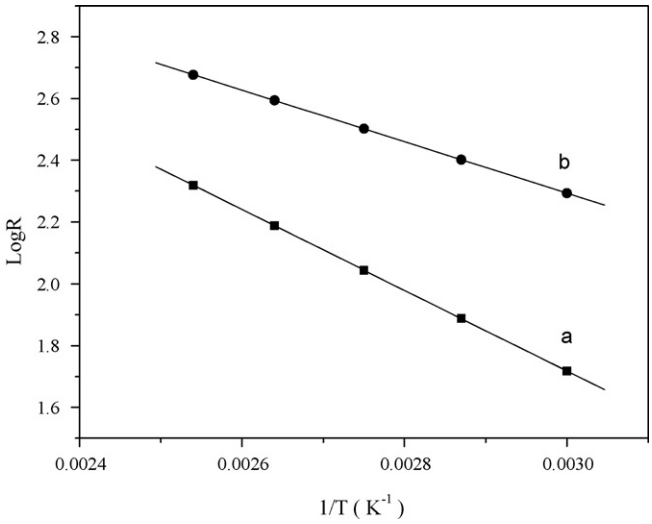

Fig. 10. Dependence of the initial hydrogenation rate over (a) amorphous Co–B particles; (b) crystallized Co–B particles on the reaction temperature. Reaction conditions: 0.25 g catalyst, 4.5 mL CMA, 40.5 mL ethanol at $PH_2 = 4.2$ MPa.

which is slightly lower than that (18 kJ/mol) obtained by Li et al. [3]. The phenomena indicated that the activity of Co sites in the Co–B catalyst was improved after being crystallized although the specific surface area decreased. It is possibly attributed to the enhanced synergistic effect between Co and B in the Co–B catalysts after being crystallized revealed by XPS (Section 3.3).

3.5.2. Hydrogenation order

Fig. 11 is the CMA hydrogenation profile over Co–B particles before and after crystallization. From Fig. 11, one can see that the products for the CMA hydrogenation over amorphous Co–B are different from those over crystallized Co–B. For amorphous Co–B, dihydrocinnamaldehyde (HCMA) and 3-phenylpropanol (HCMO) are the products. The conversion of CMA is 5% and the selectivity of HCMA and HCMO are 60% and 40%, respec-

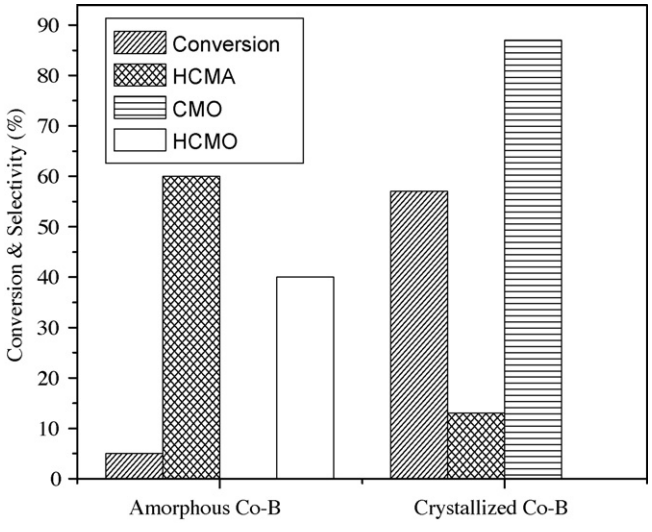

Fig. 11. CMA hydrogenation profile over Co–B particles (a) amorphous Co–B particles; (b) crystallized Co–B particles. Reaction conditions: 0.25 g catalyst, 4.5 mL CMA, 40.5 mL ethanol at $PH_2 = 4.2$ MPa and $T = 353$ K for 2 h.

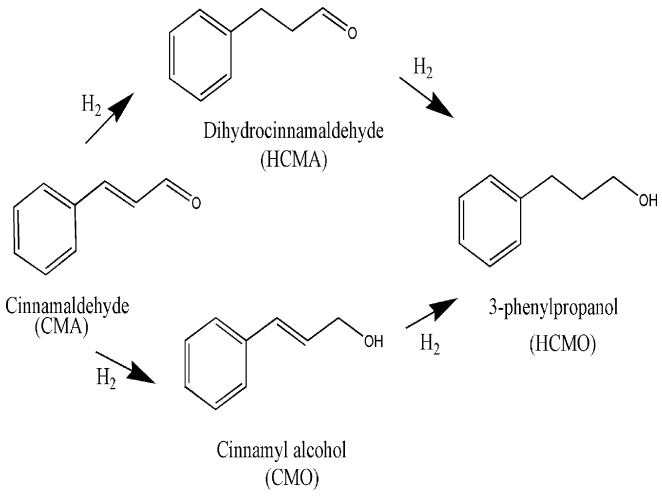

Fig. 12. Hydrogenation mechanism for CMA.

tively. According to the hydrogenation mechanism for CMA (Fig. 12), HCMO can be produced by either the hydrogenation of HCMA or cinnamyl alcohol (CMO). In order to investigate which of those routes contributed to the production of HCMO, the separate hydrogenation of HCMA and CMO was studied. The results in Fig. 13 clearly show the conversion of HCMA to HCMO reached 40% after 2 h, whereas no conversion of CMO was observed during this time period. It indicated that HCMO is produced exclusively from the hydrogenation of HCMA and not CMO. Therefore, it could be conclude that HCMA is the initial product when the CMA hydrogenation over amorphous Co–B. It further confirmed that the hydrogenation of the C=C bond is favored for amorphous Co–B particles. This result is very different from the results that CMO is the initially predominant product in the CMA hydrogenation over Co–B prepared from $CoCl_2$ reported by Li et al. [3]. The deviation is attributed to the different precursors in the preparation of catalysts.

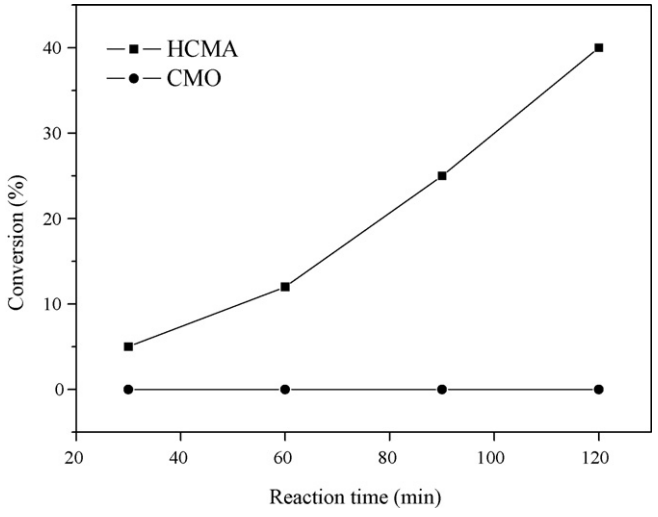

Fig. 13. Hydrogenation profile of HCMA and CMO over amorphous Co–B particles. Reaction conditions: 0.25 g catalyst, 4.5 mL HCMA or CMO, 40.5 mL ethanol at PH_2 = 4.2 MPa and T = 353 K.

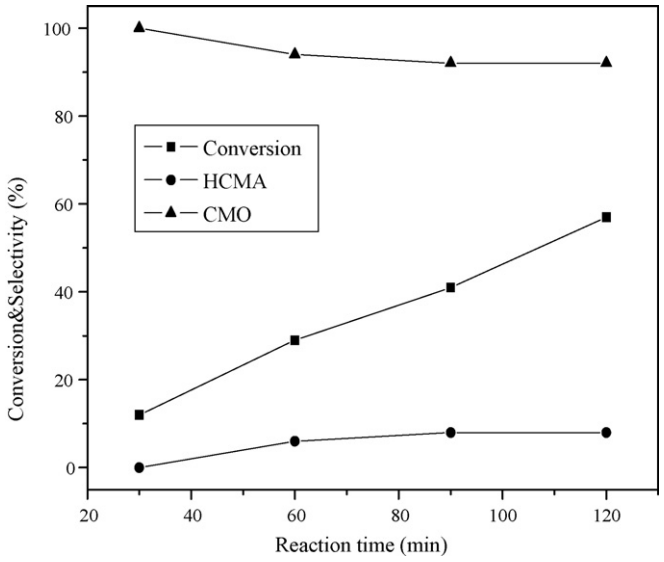

Fig. 14. Hydrogenation profile of CMA over the crystallized Co–B particles. Reaction conditions: 0.25 g catalyst, 4.5 mL CMO, 40.5 mL ethanol at PH_2 = 4.2 MPa and T = 353 K.

When the CMA hydrogenation proceeds over the crystallized Co–B particles, the products are CMO and HCMA. Furthermore, the conversion of CMA is 57%, which is considerably higher than that over amorphous Co–B. Evidently, the catalytic activity of Co–B particles is improved. It indicated that the enhanced synergistic effect between Co and B has a stronger influence on the catalytic activity of Co–B particles than that caused by the decrease of specific surface area. In addition, the selectivity to CMO is much higher than that of HCMA. In order to investigate the hydrogenation order at the beginning of the reaction, the products produced at the early stages were also analyzed. The results were shown in Fig. 14. From Fig. 14, one can see that CMO is the only product during the early stages of the CMA hydrogenation. The hydrogenation trend is similar to those reported by Li et al. [3]. The results suggested that with the promotion of crystallinity and the enhanced synergistic effect between Co and B, a vertical C=O atop geometry is preferred.

3.5.3. Hydrogenation mechanism

During the hydrogenation, the CMA can absorb onto the surface of catalysts via two competitive mechanisms [13]. One is a planar geometry through the C=C double bond, and the other through a vertical C=O atop geometry, as shown in Fig. 15.

For amorphous Co–B particles, the CMA hydrogenation may initially via a planar geometry through the C=C double bond since HCMA is the initial product. As the hydrogenation progresses, the formed product can competitively adsorb with CMA. Because of the steric effect, the adsorption of new molecules is sterically limited to vertical atop geometries. This also explains the fact that CMO is not reduced to produce HCMO whether HCMA is reduced to give HCMO.

For crystallized Co–B particles, a vertical C=O atop geometry is preferred because CMO is the only product during the early stage of CMA hydrogenation. It suggested that CMA firstly absorbed onto the surface of crystallized Co–B via a

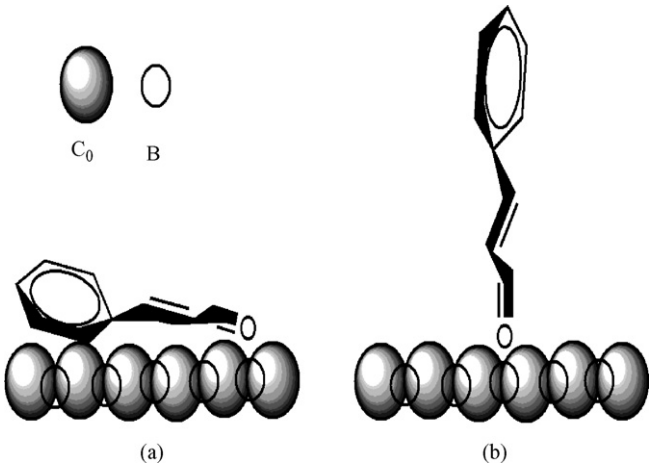

Fig. 15. Hydrogenation mechanism of CMA over Co–B particles. (a) planar geometry via C=C; (b) vertical geometry via C=O.

vertical C=O atop geometry due to the promotion of crystallinity and the enhanced synergistic effect between Co and B. The stronger affinity for the adsorption of C=O bond, which is shown in the CO temperature-programmed desorption (TPD) (Fig. 16), further confirms the hydrogenation trend to C=O bond at the early stage of CMA hydrogenation for crystallized Co–B. As the hydrogenation progresses, some CMA molecules may absorb onto the surface of crystallized Co–B via a planar C=C geometry due to the absorptive competition and then HCMA is formed.

3.6. Cycle performance

Fig. 17a and b shows the changes of conversion of CMA and selectivity of CMO during cycles for CMA hydrogenation over amorphous and crystallized Co–B, respectively. For amorphous Co–B, the conversion over three consecutive runs almost remains unchanged, then increases gradually (Fig. 17a). It is possibly attributed to that the enhancement of the synergistic effect between Co and B during the hydrogenation revealed by XPS analysis after four cycles (not shown here), which is possibly due to the enrichment of B component on the surface (Table 1), improves the activity of amorphous Co–B catalyst despite the decrease of specific surface area (Table 1). After seven cycles, the conversion reached the highest 13%, then decreased. The decrease of catalytic activity is possibly due to the dramatically decrease of specific surface area (Table 1). ICP results show that Co leaching during cycling was negligible (Table 1). In addition, the increase of selectivity for CMO during the cycle indicated that the growth of particle size is benefit to the hydrogenation to C=O in CMA, which further confirmed the hydrogenation mechanism that proposed in Section 3.5. The fact of grain growth for amorphous Co–B is also confirmed by comparison of SEM micrographs of the recycled samples (Fig. 18a and b) after several cycles with the fresh (Fig. 2a). The average particle sizes of amorphous Co–B after 4 cycles and 11 cycles are 80 and 100 nm, respectively. The evaluation for internal diffusion also suggested that the effect of internal diffusion in this work is not distinct in spite of the grain growth for amorphous Co–B during cycling.

For crystallized Co–B, the CMA conversion and CMO selectivity over 13 consecutive runs still remain unchanged (Fig. 17b).

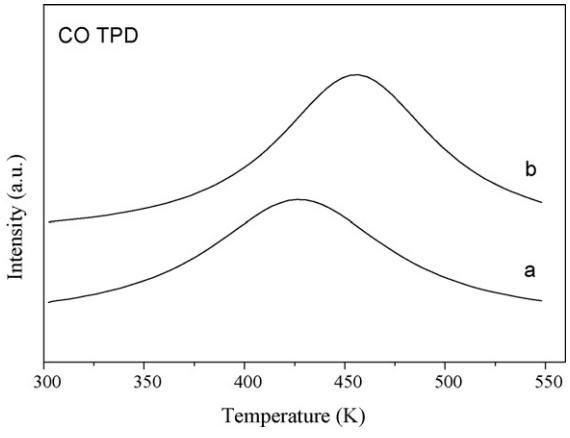

Fig. 16. CO TPD of (a) amorphous Co–B; (b) crystallized Co–B.

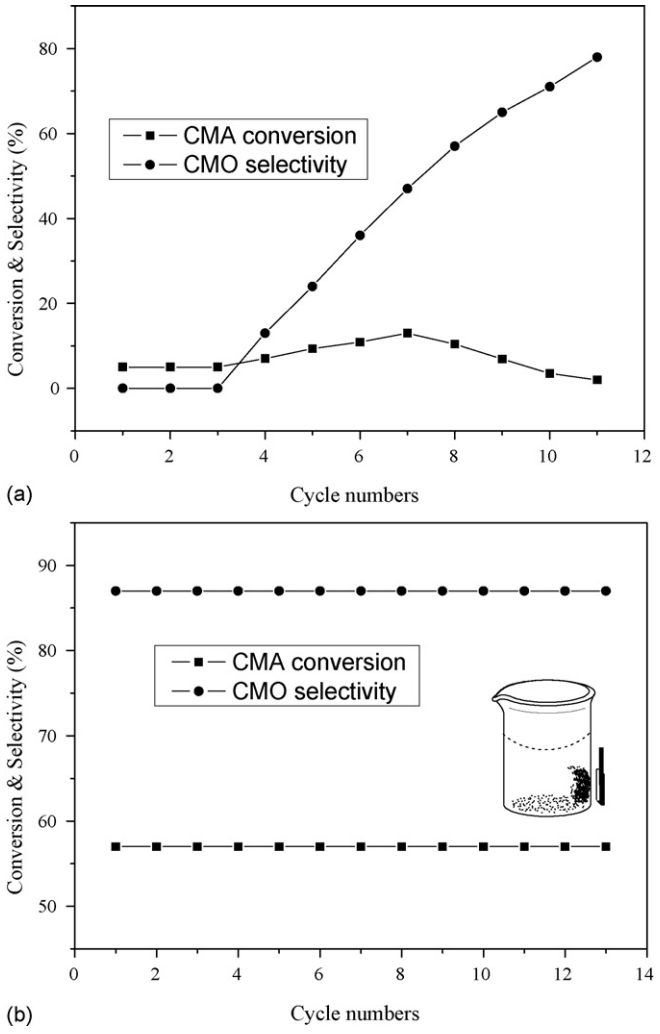

Fig. 17. The conversion of CMA and the selectivity of CMO as functions of cycle numbers over (a) amorphous Co–B particles; (b) crystallized Co–B particles (the inset is the sketch map for recycling Co–B via magnetic method). Reaction conditions: 0.25 g catalyst, 4.5 mL CMO, 40.5 mL ethanol at PH_2 = 4.2 MPa and T = 353 K for 2 h.

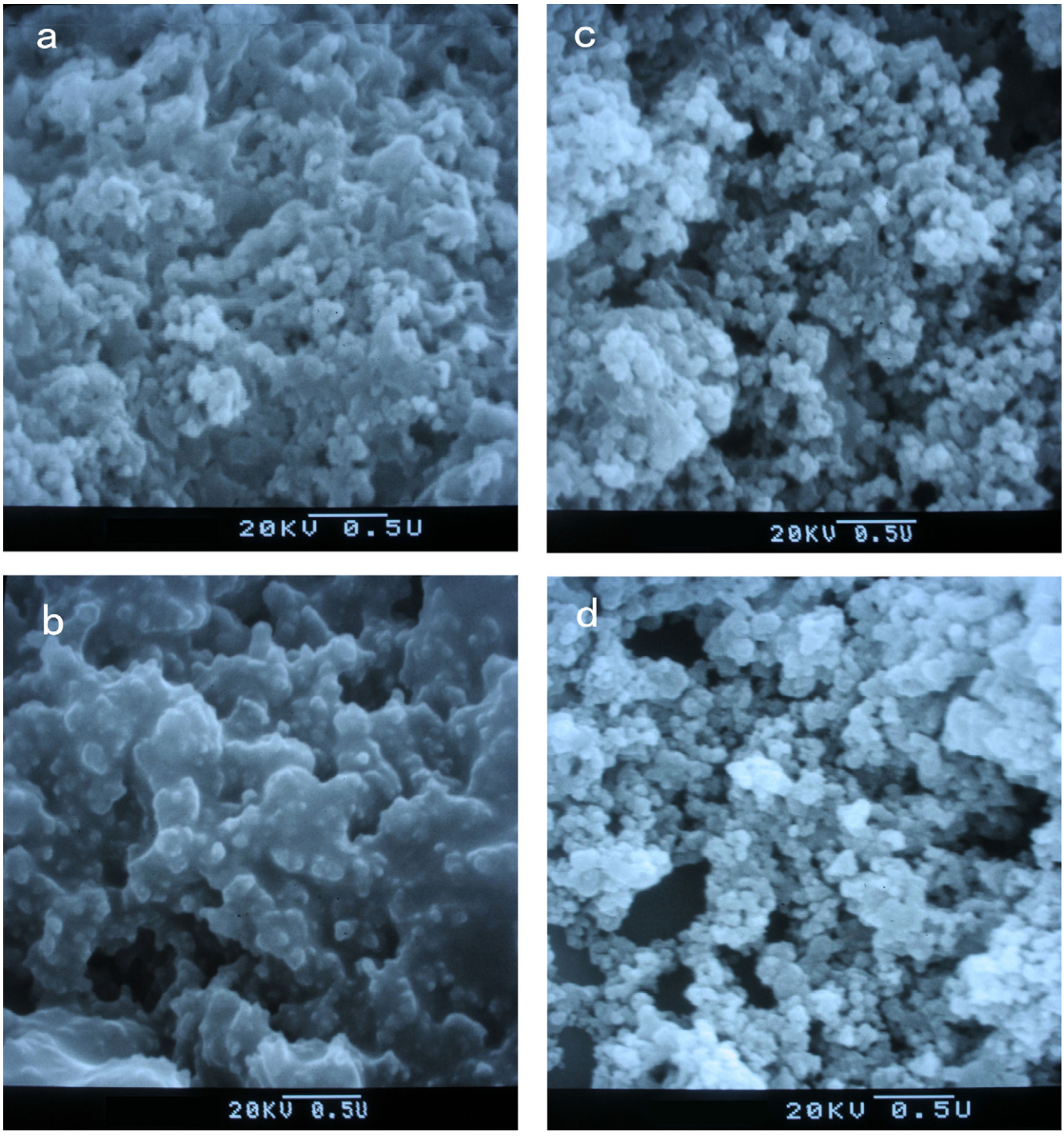

Fig. 18. Surface morphology of (a) amorphous Co–B particles after 4 cycles; (b) amorphous Co–B particles after 11 cycles; (c) crystallized Co–B particles after 6 cycles; (d) crystallized Co–B particles after 13 cycles.

The good recycle performance is attributed to its relatively stable structure confirmed by the analysis of specific surface area (Table 1) and the comparison of SEM micrographs of the recycled samples (Fig. 18c and d) after several cycles with the fresh (Fig. 2b). Because the specific surface area and particle size of crystallized Co–B almost remain unchanged during cycling. ICP results also indicate that Co leaching during cycling was negligible (Table 1). In addition, the simple recycle method, which applied the enhanced magnetic property of crystallized Co–B, also benefits it to keep the good cycle performance.

4. Conclusions

Amorphous Co–B particles were prepared from $Co(NO_3)_2$ and KBH_4. The crystallinity of Co–B is improved after low temperature ethanol-thermal treatment for 12 h without the occurrence of decomposition. The synergistic effect between Co and

B, the structure stability, and the magnetic property of Co–B enhanced while the activation energy in the CMA hydrogenation decreased after crystallization. The hydrogenation of C=C bond in cinnamaldehyde (CMA) is favored for the amorphous Co–B particles and HCMA is the initial product. With the promotion of crystallinity and the enhanced synergistic effect between Co and B, the hydrogenation of C=O bond is preferred and CMO is the only product at the hydrogenation beginning. During the cycling, the cycle performance for amorphous Co–B particles is poor due to its structure instability. But for crystallized Co–B, the CMA conversion over the crystallized Co–B still remains unchanged after 13 cycles due to its relatively stable structure and the enhanced magnetic property that make it recycle more easily.

Acknowledgements

This work was supported by the Postdoctoral Foundation of Sichuan Province (0030707602001), the National Natural Sciences Foundation of China (205903603), and 973 project of MST of China (2005CB221400). The authors thank Prof. Dai Xiaoyan and Luo Shizhong for useful discussions.

References

[1] P. Haasen, R.I. Jatte, Amorphous Metals and Semiconductors, Pergamon, London, 1986.
[2] N.F. Motte, E.A. Davis, Electronic Processes in Non-crystalline Materials, Clarendon Press, Oxford, 1979.
[3] H.X. Li, X.F. Chen, M.H. Wang, Y.P. Xu, Appl. Catal. A: Gen. 225 (2002) 117.
[4] H.X. Li, Y.D. Wu, Y. Wan, J. Zhang, W.L. Dai, M.H. Qiao, Catal. Today 93–95 (2004) 493.
[5] G.J. Zhang, Preparation Technique for Catalysts, Petrochemical Industry Publishing House of China, Beijing, 2004.
[6] Reference Manual for Operator for PHI PC Windows Software Version 1.2b, Physical Electronic Division, Perkin-Elmer.
[7] H.X. Li, H. Li, M.H. Wang, Appl. Catal. A: Gen. 207 (2001) 129.
[8] Y. Okamoto, Y. Nitta, T. Imanaka, S. Teranishi, J. Chem. Soc. Trans. 1 (1979) 2027.
[9] H. Tokoro, S. Fujii, T. Oku, J. Magn. Magn. Mater. 290 (2005) 141.
[10] V.P.M. Shati, A. Gedanken, R. Prozorov, J. Balogh, Chem. Mater. 10 (1998) 3445.
[11] D.L. Zhang, Preparation and Application Technique for Super-fine Powders, Petrochemical Industry Publishing House of China, Beijing, 2001.
[12] X.H. Guo, Kinetics for Applied Chemical Engineering, Chemistry Industry Publishing House, Beijing, 2003.
[13] J.P. Breen, R. Barch, J.G. Lopez, K. Griffin, M. Hayes, Appl. Catal. A: Gen. 268 (2004) 267.